In-situ monitoring of ultrasonic attenuation during rotating bending fatigue of carbon steel with electromagnetic acoustic resonance

HirotsuguOgi[1, 2], Takayuki Hamaguchi[1] and Masahiko Hirao[1]

[1] Graduate School of Engineering Science, Osaka University
Machikaneyama 1-3, Toyonaka, Osaka 560-8531, Japan

[2] Materials Science and Engineering Laboratory, NIST,
Boulder, Colorado 80303, USA

Keywords ultrasonics, dislocations and disclinations, metals, fatigue, resonance method

Abstract

Using electromagnetic acoustic resonance (EMAR), we studied the evolution of the surface-shear-wave attenuation and phase velocity during rotating bending fatigue of a 0.45 % C steel. In the EMAR method, we used a magnetostrictively-coupled electromagnetic acoustic transducer (EMAT) for the contactless measurements of the axial shear wave that is a surface-shear wave, propagating in a cylinder-specimen circumference direction with the axial polarization. The attenuation coefficient always showed sharp peaks around 90% of the fatigue life, independent of the fatigue-stress amplitude. In addition to the ultrasonic measurements, we made crack-growth observations using replicas and measured recovery of attenuation and velocity after stopping the cyclic loading just before and after the peak. From these results, we concluded that the evolution of the ultrasonic properties is caused by a drastic change in dislocation mobility being accompanied by the crack growth.

1. Introduction

Many studies appeared to evaluate the fatigue deterioration and the remaining life. In the ultrasonic approach, the main focus was on attenuation evolution [1, 2]. Almost all studies reported that attenuation increases slightly at the beginning, and, after experiencing a long stable period, it increases remarkably just before failure. The initial increase was attributed to the increase of the dislocation density and the final increase was attributed to the occurrence of microcracks and their subsequent growth.

The present authors recently observed a novel behavior of the surface-skimming shear-wave attenuation during rotating bending fatigue of a 0.23 % C steel pipe including a sharp attenuation peak appearing at the final stage [3]. No study reported such a peak despite the long history of research. Here, we discuss the attenuation-peak characteristics in more detail and the microstructure mechanism that produces the attenuation peak for 0.45 % C steel (1045 steel).

2. Materials

Table I shows the chemical composition. The yield strength was 420 MPa. We annealed the specimens at 300°C for 1 h before the fatigue test. The average grain size was 15 μm. We electrically polished the observing surface in a solution of 9 parts of CH_3COOH and 1 part $HClO_4$ for replica observations.

3. Measurement

Electromagnetic Acoustic Resonance (EMAR) is a contactless ultrasonic-spectroscopic technique that employs an electromagnetic acoustic transducer (EMAT) both for ultrasonic generation and reception. An EMAT directly establishes the wave sources on a metal surface and detects ultrasound through energy transduction between the mechanical vibration and electromagnetic fields, requiring no contact. Use of an EMAT thus avoids the extra energy losses associated with contact measurements, which otherwise occur in conventional measurements with piezoelectric transducers. Details of EMAR appear in Refs.4 and 5.

In this study, we used an axial shear wave [3, 6], which propagates along a cylindrical surface in the circumferential direction with the axial polarization. Figure 1 shows the magnetostrictively coupled EMAT designed for the axial shear wave in ferromagnetic materials. Operation of this EMAT is described in Ref. 6.

For a rod of radius R, we have the following frequency equation (resonant condition) for the axial shear wave: [6]

$$nJ_n(kR) - kRJ_{n+1}(kR) = 0. \quad (1)$$

Here, J_n denotes the nth Bessel function of the first kind, $k = \omega/c$ the wavenumber, ω the angular frequency, and c the shear-wave velocity. Integer n is determined by $n \sim 2\pi R/\delta$.

Here, δ denotes the meander-coil period. In the present study, n=49 and δ=0.9 mm for R=7 mm. Equation (1) provides a series of resonance frequencies $f_m^{(n)}$ with another integer m for overtones (m=1,2,3,...). The wave energy of the fundamental mode is concentrated in the outer surface region, and as the mode becomes a higher overtone, the peak amplitude moves to the inside. The fundamental mode probes a 0.5 mm-thick surface layer, the second mode has the maximum sensitivity at 0.8 mm depth, and so on. It is then possible to evaluate the radial gradient using different resonance modes. We focused on the attenuation coefficient and the phase velocity of the fundamental mode because the damage accumulation preferentially develops from the surface in the case of rotating bending fatigue.

We used a superheterodyne spectrometer to measure the resonance frequency and attenuation coefficient. The attenuation coefficient were measured by a free-decay method. Details of the measurement procedure appear in Refs. 9 and 10.

Figure 1 shows the measurement setup. The meander-line coil was wrapped around the minimum diameter of the specimen. The axial shear wave was radiated from the whole region under the coil, whose width was 20 mm. The motor rotated the specimen rod at 240 rpm (4 Hz). We attached to the specimen rod an acrylic rotor coated with copper foils, which were connected to the meander-line coil. We transmitted and received the signals using metal brushes touching the foils. The specimen, rotor, and the meander-line coil rotated together. The present system achieves *in situ* measurement of the resonance frequency and the attenuation coefficient.

All the procedures including the calculations are computerized for automatic monitoring. One set of measurements need 50 rotations, which is small enough compared with the fatigue life of 10^4 to 10^5 cycles. The bias field from the solenoidal coil was fixed at 1.4×10^4 A/m. We found no influence of the bias field on the fatigue life.

4. Result

Figure 2 shows a typical evolution of the attenuation coefficient α and the velocity v. The velocity change $(v-v_0)/v_0$ equals the resonance frequency change $(f-f_0)/f_0$, where v_0 and f_0 denote the velocity and the resonant frequency before fatiguing. We made the measurement for thirty-five steel rods with various bending stresses between 380 and 490 MPa. Fracture occurred at the minimum diameter. Common observations were as follows: (i) Over the first half the life, α is almost stable, but v monotonically decreases. (ii) Around 70% of the lifetime, α starts to decrease below the initial value. This is accompanied by an acceleration in the decrease of v. (iii) After this, α increases to a maximum and immediately drops. At the maximum, v pauses or slightly increases. (iv) Peak(s) of α always appears before failure. It is very sharp, the width being only a few percent of the life. The peak often appears twice. (V) When the bending stress was too small to cause failure, no attenuation peak appeared.

In Fig. 3, we see a close correlation between the failure cycle number (N_f) and the cycle number at which the attenuation shows a peak (N_p). When two peaks appeared,

we used the larger one to define N_p. The correlation coefficient was 0.9986 over a wide range of N_f from $3x10^4$ to $40x10^4$ cycles.

We observed the replicas taken from the specimen surface. The cracks appeared as early as about 25 % of the life. A large number of small cracks grew parallel to the circumferential direction, that is, the propagation direction of the axial shear wave. The number of cracks increased linearly throughout life, while the maximum crack length was stable until 65% of the life (less than 0.1 mm). This suggests that at an early stage, the fatigue cycles are mainly spent by the crack nucleation, not the crack growth. The crack length rapidly increased with the attenuation increase around 70 % of life.

For the recovery measurement, we stopped the fatigue test just before and after the attenuation peak, released the bending stress, and measured α and v as functions of time at room temperature. Recovery behavior was considerably different between before and after the attenuation peak. The magnitude of recovered α in 150 h relative to the previous stage was 45 % and 20 % before and after the attenuation peak, respectively. Those of v were 37 % and 17 %, respectively.

5. Discussion

Factors that could affect the ultrasonic properties during fatigue are cracks, newly created discontinuous boundaries such as the subgrain boundaries, and dislocations. The first and second factors have the effect of scattering the ultrasonic waves and cause

the apparent attenuation. The dislocations oscillate responding to the ultrasonic-wave passing with a phase lag, resulting in the absorption of the wave energy.

Obviously, cracks cause failure. Because the attenuation peak appears at the final stage and it clearly shows a correlation with the remaining life, one may regard crack initiation and growth to be the dominant mechanism behind the changes in α and v. But, we have to deny this possibility from two experimental facts: (i) Cracks fail to explain the attenuation decrease and velocity increase. (ii) Cracks fail to explain the recovery of α and v by the room-temperature aging.

We estimated the grain-scattering contribution to the attenuation coefficient [7] and obtained it to be $2\text{x}10^{-4}\ \mu\text{s}^{-1}$. This is negligible compared with the attenuation change during fatigue. Even if subgrains occur, they merely tend to decrease D and α_s.

Thus, it is natural to conclude that dislocation damping must be the dominant factor for the changes in α and v. According to the string model [8], α and v are related to the density Λ and the averaged segment length L between the pinning points of the *effective dislocations* that can move in response to ultrasonic waves by $\alpha = C_1 \Lambda L^4$ and $(v-v_0)/v_0 = -C_2 \Lambda L^2$. Here, C_1 and C_2 are positive constants. In general, the total dislocation density may saturate in the early stage of fatigue [9], and we expect no significant change in the dislocation network in the later stage. However, dislocation mobility can change even at the final stage where dislocation structure is no longer changed.

We divide the fatigue life into three stages characterized by the attenuation

evolution as shown in Fig. 3. And we attempt to explain the evolutions of α and v with the dislocation-vibration model and crack growth behavior.

In *stage I*, Λ increases because the dislocations multiply under cyclic loading, but L decreases because of the tangling. As a result, α remains nearly unchanged. At the same time, large-scale dislocation movement will occur within a very thin surface layer, including development of cell structure; and many microcracks nucleate on the surface, which can not be detected with the axial shear wave. Although we did not measure the crack depth, they are thought to be very shallow because of the work hardening of metal, radial stress gradient, and constraint to deformation below the surface. Even the fundamental mode is incapable of detecting an event occurring within such a thin surface skin. In this stage, fatigue life is spent by crack nucleation, one after another, at many scattered sites, which is supported by the replica measurements.

In *stage II*, the multiplied dislocations heavily pile up against obstacles such as grain boundaries, precipitates, and tangled dislocations. This lowers the dislocation mobility and decreases Λ and L. An attenuation depression observed before the peak supports this. In this stage, the crack length grows to several times larger than in stage I, indicating crack coalescence. Because stress concentration at the crack tip becomes remarkable with crack length, the high-stress region extends inside, which accelerates the dislocations piling up and contributes to make the dislocations immobile.

In *stage III*, the crack length drastically increases. This indicates that cracks grow downward at last to relieve the internal stress caused by the piling-up dislocations.

A large number of dislocations, which could not participate in the dislocation damping, are temporarily released from the obstacles and absorb more acoustic energy because of larger Λ and L, increasing α considerably. After that, however, these dislocations soon loose mobility by tangling and piling up to obstacles again to diminish Λ and L. Thus, α decreases and v increases as observed in stage II.

We assume that this process (dislocation tangling and piling up, crack growth inside and increase of the mobile dislocations, and again dislocation tangling and piling up) advances inside step by step and the attenuation peak emerges each time.

The interpretation above seems conjectural. But, considering that only dislocations can contribute to the observed changes of α and v, no other possible and reasonable interpretation could appear.

Dislocation-ultrasonic interaction also explains the recovery behavior. Even at room temperature, the point defects diffuse toward dislocation lines to alleviate the stress field there and create pinning points [10]. Recovery observed in the present study is understood in the same way. The difference of the recovery behavior between before and after the attenuation peak can be understood by the long dislocation segments formed immediately before the attenuation peak. Point defects will easily migrate toward the long dislocation lines without being obstructed by other point defects that have already become pinning points. The number of point defects that can reach the dislocation lines per unit time should thus be larger before the peak, resulting in a larger recover rate.

6. Conclusion

Use of a high-frequency axial shear wave is the key to confine the measurement to the damaged portion. The cycle number at the attenuation peak and the life were closely correlated, independent of the bending-stress amplitude. Changes of the attenuation coefficient and velocity caused by the fatigue recovered during aging at room temperature. This observation shows that the dominant factor contributing to their evolutions is not the presence of cracks, but dislocations. We conclude that a significant change occurs in dislocation mobility, not necessarily the whole dislocation structure, being accompanied by crack coalescence and growth inward.

Reference

[1] H. Schenck, E. Schmidtmann, and H. Kettler: *Arch. Eisenhuettenw.*, 1960, vol. 31, pp. 659-69.
[2] W. J. Bratina and D. Mills: *Canadian Metall. Quart*., 1962, vol. 1, pp. 83-97.
[3] H. Ogi, M. Hirao, and K. Minoura: *J. Appl. Phys*., 1997, vol. 81, pp. 3677-84.
[4] M. Hirao, H. Ogi, and H. Fukuoka: *Rev. Sci. Instrum*., 1993, vol. 64, pp. 3198-3205.
[5] M. Hirao and H. Ogi: *Ultrasonics*, 1997, vol. 35, pp. 413-21.
[6] H.Ogi, K. Minoura, and M.Hirao: in Review of Progress in QNDE, vol. 15, (ed. D.O.Thompson and D.E.Chimenti); 1996, New York, Plenum, pp. 1939-44.
[7] H. Ogi, M. Hirao, and T. Honda: *J. Acoust. Soc. Am*., 1995, vol. 98, pp. 458-64.
[8] A. Granato and K. Lücke: *J. Appl. Phys*., 1956, vol. 27, 583-93.
[9] M. Klesnil and P. Lukáš: 'Fatigue of Metallic Materials'; 1980, New York, Elsevier.
[10] A. H. Cottrell and B. A. Bilby: *Proc. Phys. Soc*., 1949, vol. A 62, 49-62.

Table I. Chemical composition of 1045 steel in mass % (balance Fe).

C	Si	Mn	P	S	Cu	Ni	Cr
0.48	0.18	0.78	0.012	0.024	0.05	0.03	0.11

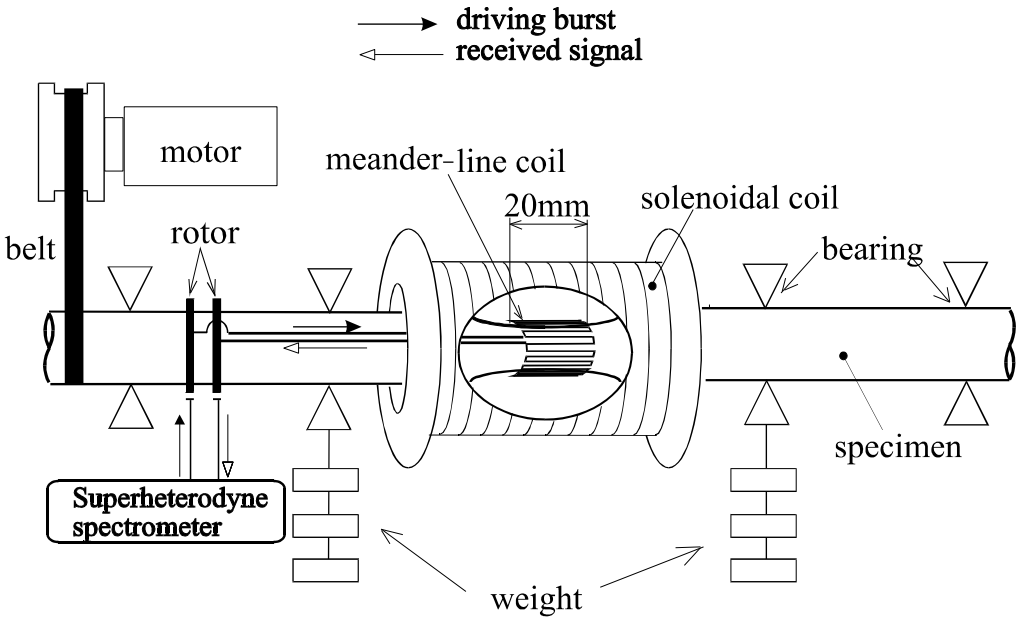

Fig. 1 Magnetostrictively coupled EMAT for axial shear wave and the measurement setup.

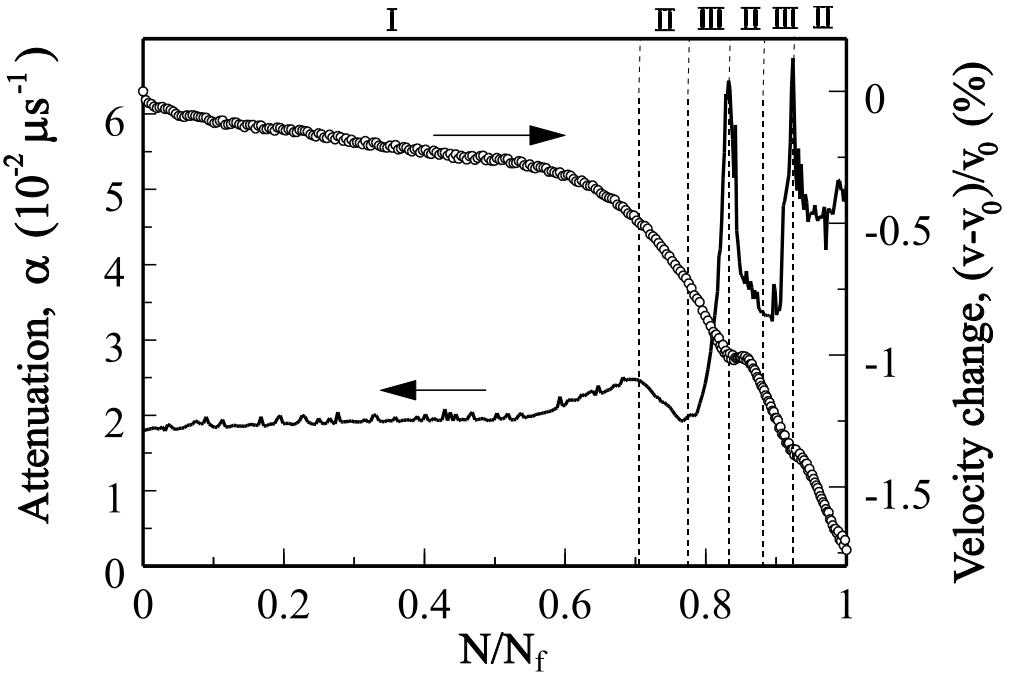

Fig. 2 Typical evolutions of the attenuation coefficient and the velocity change of the fundamental mode. The stress amplitude is 440 MPa and the fatigue life N_f = 61,600.

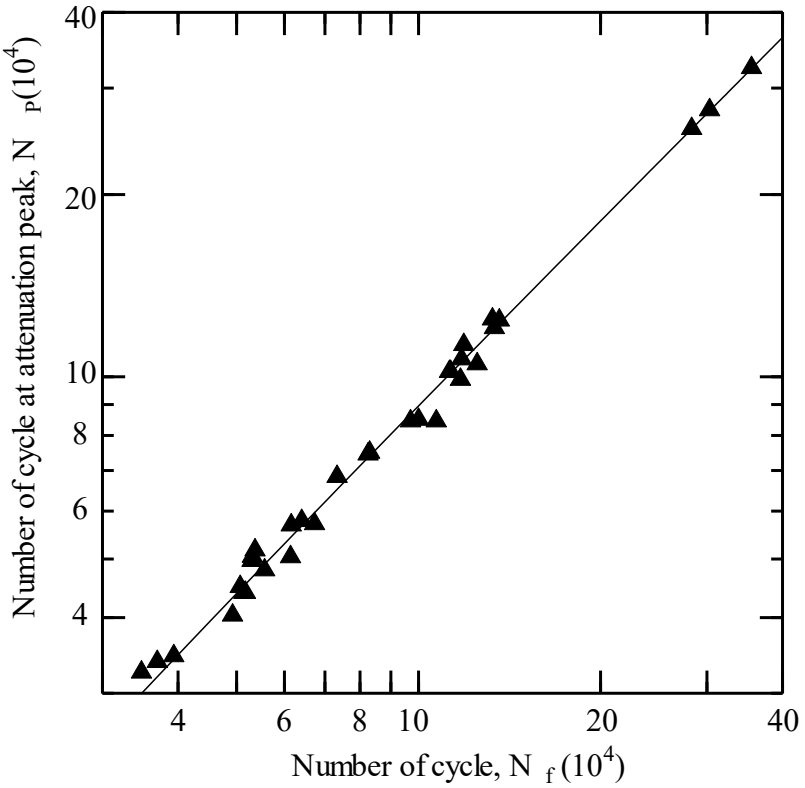

Fig. 3 Relationship between the attenuation-peak cycle number N_p and the fatigue life N_f.